A laser-locked hollow waveguide gas sensor for simultaneous measurements of CO_2 isotopologues with high accuracy, precision and sensitivity

Yang Liu,[†] Tao Wu, *,[†] Qiang Wu,[‡,†] Weidong Chen,[§] Chenwen Ye,[†] Mengyu Wang,[†] Xingdao He[†]

[†]Key Laboratory of Nondestructive Test (Ministry of Education), Nanchang Hangkong University, Nanchang, 330063, China

[‡]Department of Mathematics, Physics and Electrical Engineering, Northumbria University, Newcastle upon Tyne, NE1 8ST, UK

[§]Laboratoire de Physicochimie de l'Atmosphère,Université du Littoral Côte d'Opale 189A, Av. Maurice Schumann, Dunkerque 59140, France

*E-mail: wutccnu@nchu.edu.cn

ABSTRACT: A laser frequency locked hollow waveguide (HWG) gas sensor is demonstrated for simultaneous measurements of three isotopologues ($^{12}CO_2$, $^{13}CO_2$, and $^{18}OC^{16}O$) using wavelength modulation spectroscopy (WMS) with a 2.73 μm distributed feedback (DFB) laser. The first harmonic (1*f*) signal at the sampling point where the peak of the second harmonic (2*f*) signal located was employed as locking point to lock the laser frequency to the transition center of $^{13}CO_2$, while the absorption lines of $^{12}CO_2$ and $^{18}OC^{16}O$ were being scanned. Continuous measurements of three isotopologues of 4.7% CO_2 samples over 103 minutes under free running and frequency locking conditions were performed, respectively. The measurement accuracy and precision of the three isotopologues achieved under frequency locking condition were at least 3 times and 1.3 times better than those obtained under free running condition. The Allan variance plot of the developed laser-locked HWG gas sensor shows a detection limit of 0.72 ‰ for both $\delta^{13}C$ and $\delta^{18}O$ under the frequency locking condition with a long stability time of 766 s. This study demonstrated the high potential of a novel human breath diagnostic sensor for medical diagnostic with high accuracy, precision, sensitivity, and without frequently repeated calibration.

Breath analysis has been considered as an effective, non-invasive way to in-vitro monitor various physiological and pathological processes in the human body. Compared to traditional offline analysis, real-time breath analysis possessing fast gas exchange and data acquisition enables to provide spatially resolved information of specific metabolic process [1]. To date, there are more than 2000 respiratory gases ranging from parts per trillion (ppt) to tens of percent (%) in concentration, identified to be present in exhaled human breath, some of which have been proven to be useful biomarkers for diagnosing certain physical conditions and diseases [2]. Carbon dioxide is not only among the most abundant components in breath, but also their concentrations in exhaled breath offer important information of the metabolic status of a patient. The ^{13}C-isotope of CO_2 in the exhaled gas has been demonstrated for diagnosis of Helicobacter pyroli infection, liver malfunction, small intestinal bacterial overgrowth, fat absorption, pancreatic insufficiency, sepsis, and gastric emptying [3]. The ^{16}O isotope in $^{12}CO_2$ and ^{18}O isotope in body water ($H_2{}^{18}O$) are rapidly interchanged during the respiration process in humans. Recently, ^{18}O-isotope of CO_2 is also found being used as a potential biomarker to distinctively track the pathogenesis of Helicobacter pylori [4]. While measurement precision of ^{13}C or ^{18}O better than 1‰ is demanded for practical clinical applications [4], when a relative change of $\delta^{13}C$ and $\delta^{18}O$ in human breath samples monitored before and after ingestion of ^{13}C-labeled substance is quantified. These applications promote the development of novel experimental techniques capable of performing real time measurement of isotope ratios with high accuracy, precision and sensitivity.

With unique advantages in sensitivity and specificity, various spectroscopic techniques, including Fourier transform infrared spectroscopy (FTIR) [5], photoacoustic spectroscopy (PAS) [6], tunable diode laser absorption spectroscopy (TDLAS) [7], cavity ring-down spectroscopy (CRDS) [8], and off-axis integrated cavity output spectroscopy (OA-ICOS) [9], have been developed extensively for measurements of absorption of CO_2 isotopes in human breath in the near-infrared (NIR) and especially in the mid–infrared (MIR), where the absorption line strength of CO_2 isotopes is at least 100 times stronger than that in the NIR. To achieve sufficient sensitivity for spectroscopic measurement of isotopes, different types of multi-pass cells (e.g. Herriott cell and White cell) and high finesse optical cavities were used to increase the effective absorption path length, which are usually combined with wavelength modulation spectroscopy (WMS) to remove spectrum background and decrease the 1/*f* noise. However, these cells and cavities are usually bulky and the optical alignment is quite critical. Alternative way of increasing the effective absorption path length is to employ hollow waveguide (HWG) fiber or hollow-core fiber (HCF) filled with the gas of interest [7, 10-12]. Such fiber

enables low-loss light propagation in the MIR spectral regions, its extended optical path (~ m) and small sampling volume (~ mL) guarantee high sensitivity and fast response time for gas concentration measurement. Unfortunately, multimode propagation and scattering on inner reflective coating both may cause optical fringes, which are also sensitive to environmental temperature, current and mechanical fluctuations, leading to decrease the measurement sensitivity [13-14]. In addition, frequency shift in a free running DFB diode laser due to ambient environmental fluctuations degrades the stability of the laser system. This issue is usually solved by employing laser frequency locking method. In conventional laser frequency locking method, a highly stabilized external reference cell is needed [15-17]. The modulated light transmitted through the reference cell is collected with a photodetector, 1*f* or 3*f* signal at the central wavelength of target gas absorption line is measured as an error signal for locking the laser wavelength to the target absorption line center, and 2*f* signal at the locked wavelength is used to infer the gas concentration. If the whole absorption line is required for scanning, high finesse optical cavity and sophisticated PDH (Pound-Drever-Hall) frequency-locking technology and/or optical feedback (OF)) are usually needed for laser frequency locking.

In this work, we present a laser-locked hollow waveguide gas sensor for measurements of three CO_2 isotopologues ($^{13}CO_2$, $^{12}CO_2$, and $^{18}OC^{16}O$). Laser frequency locking was employed to suppress optical fringes specified in fiber and drift in laser frequency. The use of WMS, involving a 2.73 μm DFB laser to cover the strong absorptions of three CO_2 isotopologues, coupled to a 5 m HWG cell with a small volume (3.9 mL) enabled CO_2 isotopologues detection with high sensitivity and time-resolution. Higher performance in terms of measurement accuracy and precision was demonstrated in comparison with free running laser system. Lower detection limit of $\delta^{13}C$ and $\delta^{18}O$ was achieved under the frequency locking condition.

The WMS-2*f* theory has been previously detailed [18] and is only briefly recalled here. For 2f signals' detection, the Fourier coefficient of $S_{2f}^{in}(\bar{\nu}_d,\bar{\nu}_a)$ signal for a Lorentzian lineshape can be written as [19]

$$S_{2f,L}^{in}(\bar{\nu}_d,\bar{\nu}_a) = -\beta\eta I_0 S n_a L \chi_{2f,L}^{even}(\bar{\nu}_d,\bar{\nu}_a) \quad (1)$$

where $\bar{\nu}_d$ and $\bar{\nu}_a$ are width-normalized center detuning (given by $\nu_d/\Delta\nu_L$ for the Lorentzian case, ν_d is the detuning frequency) and modulation amplitude (given by $\nu_a/\Delta\nu_L$, ν_a is the modulation amplitude), respectively. $\Delta\nu_L$ is the half width at half maximum (HWHM) of the Lorentzian profile, β is the gain of the lock-in amplifier, η is the instrumentation factor, I_0 is the power of incident light, S is the line strength of the transition, n_a is the density of absorbers, L is the path length, and $\chi_{2f,L}^{even}(\bar{\nu}_d,\bar{\nu}_a)$ is the 2*f* of the area-normalized Lorentzian lineshape function [19]. When $\bar{\nu}_d$ =0, the 2*f* amplitude $S_{2f,L}^{in}(0,\bar{\nu}_a)$ can be written as

$$S_{2f,L}^{in}(0,\bar{\nu}_a) = -\beta\eta I_0 S n_a L \chi_{2f,L}^{even}(0,\bar{\nu}_a) \quad (2)$$

where the 2f amplitude of Lorentzian lineshape function $\chi_{2f,L}^{even}(0,\bar{\nu}_a)$ can be derived as [20]

$$\chi_{2f,L}^{even}(0,\bar{\nu}_a) = \frac{2}{\sqrt{1+(\bar{\nu}_a)^2}}\left(\frac{1-\sqrt{1+(\bar{\nu}_a)^2}}{1+\sqrt{1+(\bar{\nu}_a)^2}}\right) \quad (3)$$

The parameters like β, η, S, and L in equation (2) are fixed. For constant modulation amplitude and pressure in the gas cell, $\chi_{2f,L}^{even}(0,\bar{\nu}_a)$ is also constant. If the laser intensity I_0 is unchanged during the measurement, the 2*f* amplitude $S_{2f,L}^{in}(0,\bar{\nu}_a)$ is linearly proportional to the gas concentration n_a. However, the laser intensity I_0 is related to laser frequency, which is susceptible to environmental fluctuation, especially for tubular optical waveguide. Hence, laser frequency locking technique is highly desired for HWG gas sensor to achieve robust, high accuracy and high sensitivity gas concentration measurements.

If laser current is driven through a sawtooth wave signal overlapped with a high-frequency sine wave signal, 2*f* signals of three CO_2 isotopologues are acquired as a function of sampling point using a data acquisition card. When laser frequency is drift, the sampling points corresponding to 2*f* signal peaks of three CO_2 isotopologues change. Hence, the 1*f* signal of one CO_2 isotopologues at the sampling point where the peak of 2*f* signal located is employed as locking point to lock the laser frequency to the transition center of this CO_2 isotopologues. Once the absorption peak of one CO_2 isotopologues is locked, the positions of 2*f* peaks of all three CO_2 isotopologues are fixed.

Isotopic ratios are commonly expressed as 'δ-value', which is usually expressed in per mil (‰). For the $^{12}C/^{13}C$ and $^{18}O/^{16}O$ ratios in CO_2, the $\delta^{13}C$ and $\delta^{18}O$ values are defined as follows [21]

$$\delta^{13}C = \delta^{13}C_{cal} + \frac{R_{sam} - R_{cal}}{R_{VPDB}^{13}} \quad (4)$$

$$\delta^{18}O = \delta^{18}O_{cal} + \frac{R_{sam} - R_{cal}}{R_{VPDB-CO2}^{18}} \quad (5)$$

where R_{sam} and R_{cal} denotes the concentration ratios of $^{13}CO_2/^{12}CO_2$ and $^{18}OC^{16}O/^{16}OC^{16}O$ for gas samples and calibration gas, respectively. R_{VPDB}^{13} and $R_{VPDB-CO2}^{18}$ refer to the Vienna Pee Dee Belemnite (VPDB) scale.

EXPERIMENTAL SECTION

The schematic of the experiment system is depicted in Figure 1 (a). A DFB laser (Nanoplus GmbH) operating at 2.73 μm with a 11.2 mW maximum output power was employed as the light source to probe three CO_2 isotopologues absorption lines. The laser device is integrated in a TO5 package together with a thermoelectric cooler (TEC) and collimated with an aspheric lens. The laser beam was focused into the input of a 5-m-long HWG (HWEA 10001600, Polymicro Technologies, USA) with a lens with a focal length of 75 mm. The HWG has a hollow-core diameter of ~1000 μm, optically transparent from 2.6 to 10.6 μm with a max bending loss of 1.5 dB/m. The HWG fiber is fixed in custom-designed splice and sealed by silicon glue, the schematic layout of the splice was reported in reference [11].The light out of the HWG was received with a photovoltaic detector (PVI-4TE-10.6, VIGO System S.A). The laser, focusing lens, and photodetector were arranged as close to the HWG as possible to minimize the possible interference of CO_2 absorption outside the HWG. The injection current and the temperature of the DFB laser were provided using a commercial diode laser driver (LDC-3724, ILX Lightwave). A high-frequency (10 kHz), low-amplitude (90 mV rms) sine wave signal generated from a lock-in amplifier (SR830, Stanford Research System) and a sawtooth wave signal with

peak to peak value of 1.2 V and frequency of 10 Hz provided by a function generator were superimposed using an adder and sent to a proportional integral servo controller (LB-1005, new focus). The output of the PID controller was sent to the current modulation port of the laser controller to drive the laser. The signals detected by the photodetector were sent to two lock-in amplifiers for 1*f* and 2*f* demodulation, respectively. The 1*f* signal from one lock-in amplifier was used for monitoring the drift of the laser frequency, and the 2*f* signal from another lock-in amplifier was used for gas concentration retrieval. Both 1*f* and 2*f* signal were acquired with a 14-bit analog-to-digital data acquisition card (DAQ-2010, ADlink, China) at a sampling rate of 40 kHz. The acquired 1*f* and 2*f* signal were further processed with a self-written LabWindows program, and then the produced error signal was sent to the error port of the PID controller to lock the laser frequency to the line center of the absorption feature. Two mass flow controllers (MFC) were placed at the outlet of CO_2 and nitrogen cylinders to control the flow rate of two gases for CO_2 dilution. The concentrations of diluted CO_2 samples were determined by setting different flow rates of two MFCs. The diluted standard CO_2 samples were pumped into the HWG through a third MFC. The pressure in the HWG gas cell was maintained with a pressure controller (640B, MKS Instruments, USA). The HWG was coiled parallel on the surface of a plastic ring with a diameter of 300 mm manufactured by 3D printing, and then covered with silver foil, heater band and insulation foam, successively (Figure 1(b)).The HWG temperature was stabilized at 30 °C using a heating belt and a platinum resistor (Pt100), which were controlled via a PID temperature controller. It is noted that although the condensation from exhaled breath might be absorbed on the fiber inner wall, the measurement in our experiments was performed in low pressure and dynamic way which can effectively mitigate the water vapor condensation effect [7, 11].

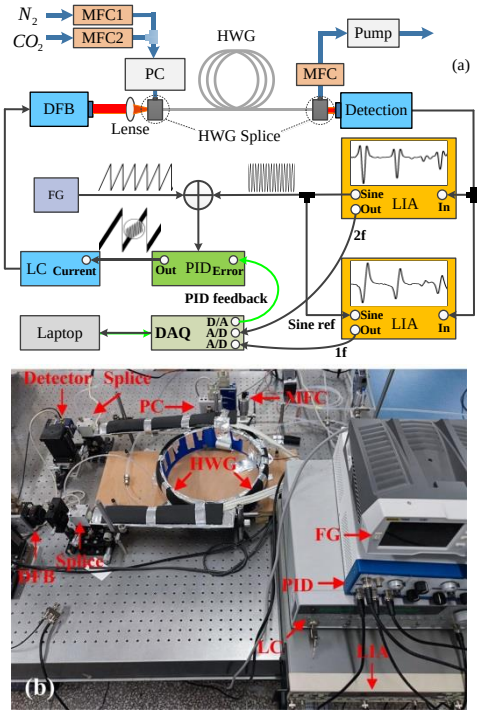

Figure 1 (a) Schematic of laser frequency locking based HWG gas sensor; (b) photograph of the optical layout of the prototype HWG gas sensor. DFB, distributed feedback laser; FG, function generator; LC, laser controller; PID, proportional-integral-derivative controller; LIA, lock-in amplifier; DAQ, data acquisition card; MFC, mass flow controller.

The central wavelength of the laser was adjusted to near the $^{18}O^{12}C^{16}O$ absorption peak with a temperature and a current of the diode laser set at 34 °C and 134 mA, respectively. laser tuning from 3660.60562 to 3661.55796 cm^{-1} allowed covering three absorption lines of $^{12}C^{16}O_2$ (3661.4948 cm^{-1}), $^{18}O^{12}C^{16}O$ (3661.0836 cm^{-1}) and $^{13}C^{16}O_2$ (3660.7696 cm^{-1}). Typical spectra of the 1*f* and 2*f* signals of the three CO_2 isotopologues in a 4.7% CO_2 sample at 200 Torr, after wavelet denoising, are shown in Figure 2. The sample point corresponding to the 2*f* signal peak of $^{13}C^{16}O_2$ (nominated as reference point in Figure 2) was recorded by LabWindows program during every scan. The corresponding 1*f* signal at this sample point was employed as locking point and also recorded during every scan. The locking point recorded during the first scan named as the first locking point. The amplitude difference between each locking point and the first locking point was used as the error signal, which was sent to the PID controller for locking the laser frequency to the transition center of $^{13}C^{16}O_2$.

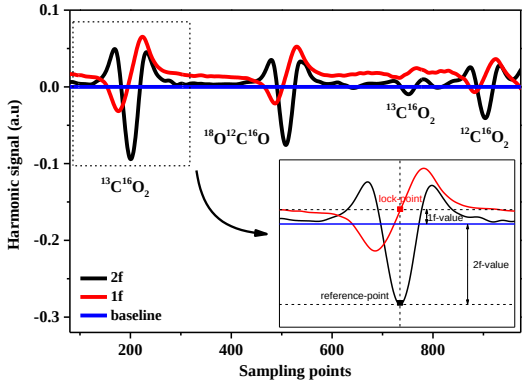

Figure 2 Schematic of 1*f* (red line) and 2*f* (black line) signals of three CO_2 isotopologues for frequency locking. Inset figure: 1*f* and 2*f* signals of $^{13}C^{16}O_2$, the red square denotes the locking point, the black square denotes the reference point.

RESULTS AND DISCUSSION

In order to obtain the largest 2*f* peak values, laser modulation parameters (modulation amplitude and modulation frequency) and pressure in the HWG were all optimized [14].

In order to retrieve unknown concentrations of three isotopologues $^{12}CO_2$, $^{13}CO_2$, and $^{18}OC^{16}O$, the relationship between 2*f* peak values and three isotopologues concentrations need to be calibrated. For CO_2 isotopic ratio measurements in human breath, CO_2 concentrations in the range of 2-6% is expected [21]. Six CO_2 samples at different concentrations (2%, 2.9%, 3.8%, 4.7%, 5.7%, 6.4%) have been prepared by dynamic dilution of pure CO_2 gas with high-purity nitrogen gas. A plot of measured 2*f* peak values versus different concentrations of three CO_2 isotopologues was shown in Figure 3. Figure 3 shows the fitted curves had very good linearities for $^{13}CO_2$, $^{12}CO_2$, and $^{18}OC^{16}O$ with a linear correlation of 0.9983, 0.9994, and 0.9998 respectively, which were used as calibration function to determine CO_2 isotopologues concentrations.

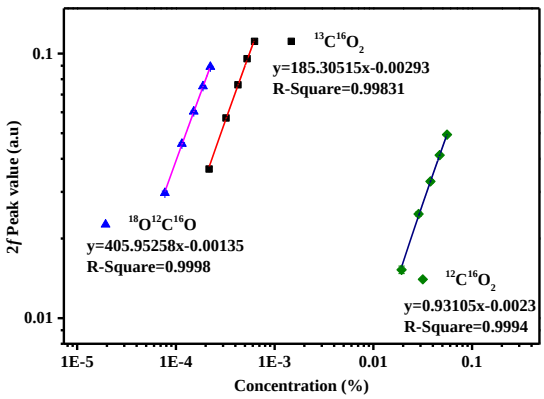

Figure 3 2*f* peak values as function of the CO_2 isotopologues concentrations.

Another important parameter, the response time of the laser-locked HWG gas sensor, was then investigated through the measurements of the seven different $^{13}CO_2$ concentrations prepared and shown in Figure 4. The sampling gas flow rate to the HWG cell was keep constant at 17 mL/s. The 0–10% delay time τ_d in rising and falling process was around 2 s, while the 10–90% response times τ_r in rising and falling process were 9.6 and 13.5 s, respectively. The inlet perfluoroalkoxy (PFA) tube before the HWG had a length of 130 cm and an inner diameter of 4.35 mm, which was used for gas diffusion and mixture totally in the inlet tube. The HWG provided a gas sampling volume of only 3.9 mL however the inlet tube occupied a volume of 19 mL which dominated the sensor response time in the present work.

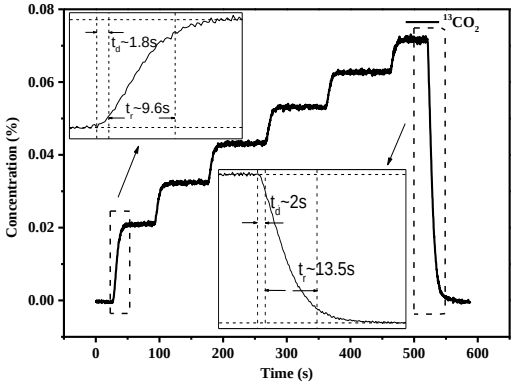

Figure 4 Response time for the HWG gas sensor.

Performance comparison of the HWG gas sensor under free-running (lock off) and frequency locking (lock on) condition has been performed. Continuous measurements of 4.7% CO_2 gas samples were carried out over 103 minutes with a rate of 0.29 s per spectrum under two different conditions at a pressure of 200 Torr and a gas flow rate of 17 mL/s to the HWG cell. The measured 2*f* peak values were transformed to concentration according to the calibration curve shown in Figure 3. Figure 5 shows the fluctuation of measured CO_2 isotope concentrations under free running and frequency locking conditions. An obvious drift of the measured concentrations of three CO_2 isotopologues compared to predicted concentrations can be observed under free running condition, while the measured concentrations of three CO_2 isotopologues are close to the predicted concentrations under frequency locking condition. The measured average concentration values of $^{12}C^{16}O_2$, $^{13}C^{16}O_2$ and $^{18}O^{12}C^{16}O$ under free running condition were 4.83 %, 536.87 ppmv and 195.10 ppmv, with relative uncertainties of 3.0%, 2.0% and 3.8%, respectively. 1σ measurement precisions were 0.063 %, 6.97 ppmv and 2.65 ppmv for $^{12}C^{16}O_2$, $^{13}C^{16}O_2$ and $^{18}O^{12}C^{16}O$, respectively. For frequency locking condition, the measured average concentration values of $^{12}C^{16}O_2$, $^{13}C^{16}O_2$ and $^{18}O^{12}C^{16}O$ were 4.69 %, 528.60 ppmv and 189.15 ppmv, with relative uncertainties of 0.1%, 0.4% and 0.6%, respectively. 1σ measurement precisions of $^{12}C^{16}O_2$, $^{13}C^{16}O_2$ and $^{18}O^{12}C^{16}O$ were 0.049 %, 3.08 ppmv and 1.51 ppmv, respectively. The measurement accuracy and precision were improved at least 3 times and 1.3 times using frequency locking approach in comparison to free running condition. The discontinuation in the long-term measurement results of $^{13}C^{16}O_2$ and $^{18}OC^{16}O$ between laser "lock off" and "lock on" was due to the setting of optimal locking parameters.

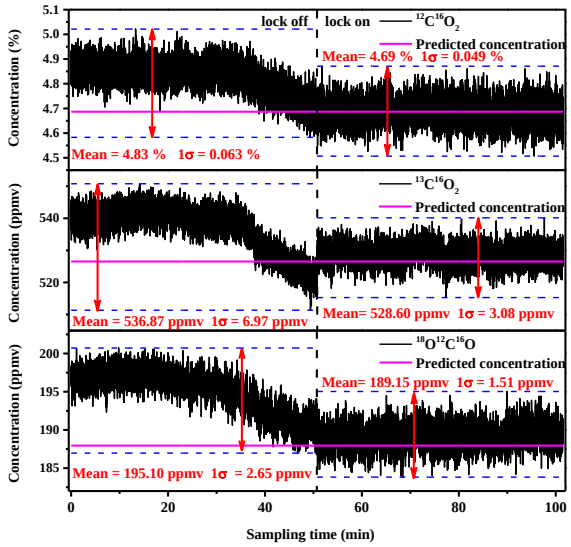

Figure 5 Long-term measurement results in two operation modes for the developed HWG-based sensor.

The stability time and detection limits of the HWG gas sensor were evaluated using Allan variance analysis. As shown in Figure 6, the Allan deviation decreases with the integration time τ in the form of $\tau^{-1/2}$. The Allan variance plot shows the detection limit of both $\delta^{13}C$ and $\delta^{18}O$ under frequency locking condition was the same of 0.72‰, corresponding to a long stability time of 766 s in which the white noise is dominant in the measurements.

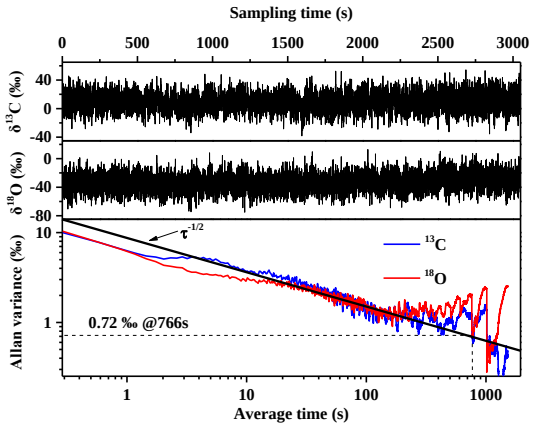

Figure 6 Measured $\delta^{13}C$ and $\delta^{18}O$ results in frequency locking mode. The Allan variance plot shows the detection limit at the optimal integration time.

CONCLUSIONS

In this work, a laser-locked HWG gas sensor was developed for simultaneous concentration measurement of three isotopologues of $^{12}C^{16}O_2$, $^{13}C^{16}O_2$ and $^{18}O^{12}C^{16}O$ with improved accuracy, precision and sensitivity compared to free running system.

Through near two hours measurements, the concentration of $^{12}C^{16}O_2$, $^{13}C^{16}O_2$ and $^{18}O^{12}C^{16}O$ were recorded and compared between free running and frequency locking modes. None drift of the concentrations of $^{12}C^{16}O_2$, $^{13}C^{16}O_2$ and $^{18}O^{12}C^{16}O$ under frequency locking was found. The relative uncertainties of $^{12}C^{16}O_2$, $^{13}C^{16}O_2$ and $^{18}O^{12}C^{16}O$ under free running condition were 3.0%, 2.0% and 3.8%, respectively. 1σ measurement precisions were 0.063 %, 6.97 ppmv and 2.65 ppmv for $^{12}C^{16}O_2$, $^{13}C^{16}O_2$ and $^{18}O^{12}C^{16}O$, respectively. For frequency locking condition, the relative uncertainties of $^{12}C^{16}O_2$, $^{13}C^{16}O_2$ and $^{18}O^{12}C^{16}O$ were improved to be 0.1%, 0.4% and 0.6%, with 1σ measurement precisions of 0.049 %, 3.08 ppmv and 1.51 ppmv, respectively. At least 3 times and 1.3 times improvement for the measurement accuracy and precision were achieved by the frequency locking approach compared to free running approach. The Allan variance plot gives the detection limit of $\delta^{13}C$ and $\delta^{18}O$ under frequency locking condition were both 0.72‰ at an optimal integration time of 766 s. This work demonstrates the potential of the laser-locked HWG gas sensor for non-invasive human breath real-time diagnostic, as well as several research fields, including ecology [22], atmospheric chemistry [23] and geochemistry [24].

AUTHOR INFORMATION

Corresponding Author

Tao Wu - *Key Laboratory of Nondestructive Test (Ministry of Education), Nanchang Hangkong University, Nanchang, 330063, China*; E-mail: wutccnu@nchu.edu.cn

Authors

Yang Liu, Chenwen Ye, Mengyu Wang, Xingdao He - *Key Laboratory of Nondestructive Test (Ministry of Education), Nanchang Hangkong University, Nanchang, 330063, China*

Qiang Wu - *Department of Mathematics, Physics and Electrical Engineering, Northumbria University, Newcastle upon Tyne, NE1 8ST, UK*

Weidong Chen - *Laboratoire de Physicochimie de l'Atmosphère, Université du Littoral Côte d'Opale 189A, Av. Maurice Schumann, Dunkerque 59140, France*

Notes

The authors declare no competing financial interest.

ACKNOWLEDGMENT

The authors acknowledge the support of the National Natural Science Foundation of China (Grant No. 42175130, 61965013, 61865013), the Key Research and Development Program of Jiangxi Province, China (20203BBG73039), the National Key Research and Development Program of China (No.2018YFE0115700) and Postgraduate Innovation Foundation of Nanchang Hangkong University (YC2020078).

REFERENCES

(1) Metsälä M.; Schmidt F. M.; Skyttä M.; Vaittinen O.; and Halonen L. Acetylene in breath: background levels and real-time elimination kinetics after smoking. *J. Breath Res.* **2010**, *4*, 046003.

(2) Amann, A.; Smith, D., Eds. Volatile Biomarkers: Non-Invasive Diagnosis in Physiology and Medicine; Elsevier: Amsterdam, The Netherlands, **2013**.

(3) Modak, A. S. ^{13}C breath tests: transition from research to clinical practice. In Breath Analysis for Clinical Diagnosis and Therapeutic Monitoring, Amann A. and Smith D. Eds., World Scientific: Singapore, **2005**, 457–478.

(4) Som, S.; De, A.; Banik, G. D.; Maity, A.; Ghosh, C.; Pal, M.; Daschakraborty, S. B.; Chaudhuri, S.; Jana S; Pradhan, M. Mechanisms linking metabolism of Helicobacter pylori to ^{18}O and ^{13}C-isotopes of human breath CO_2. *Sci. Rep*. **2015**, *5*, 10936.

(5) Seichter, F.; Wilk, A.; Wörle, K.; Kim, S; Vogt, J.; Wachter, U.; Radermacher, P.; Mizaikoff, B. Multivariate determination of $^{13}CO_2/^{12}CO_2$ ratios in exhaled mouse breath with mid-infrared hollow waveguide gas sensors. *Anal. Bioanal. Chem.* **2013**, *405*, 4945–4951.

(6) Wang, Z.; Wang, Q.; Ching, J. Y. L.; Wu, J. C. Y.; Zhang, G.; Ren, W. A portable low-power QEPAS-based CO_2 isotope sensor using a fiber-coupled interband cascade laser. *Sensor Actuat. B: Chem*. **2017**, *246*, 710-715.

(7) Zhou, T.; Wu, T.; Wu, Q.; Ye, C.; Hu, R.; Chen, W.; He, X. Real-time measurement of CO_2 isotopologue ratios in exhaled breath by a hollow waveguide based mid-infrared gas sensor. *Opt. Express* **2020**, *28*, 10970-10980.

(8) Crosson E. R.; Ricci K. N.; Richman B. A.; Chilese F. C.; Owano T. G.; Provencal R. A.; Todd M. W.; Glasser J.; Kachanov A. A.; Paldus B. A.; Spence T. G.; Zare R. N. Stable isotope ratios using cavity ring-down spectroscopy: determination of $^{13}C/^{12}C$ for carbon dioxide in human breath. *Anal. Chem*. **2002**, *74*, 2003–2007.

(9) Han, L.; Xia H.; Pang, T.; Zhang, Z.; Wu, B.; Liu S.; Sun, P.; Cui, X.; Wang, Y.; Sigrist, M.; Dong, F.;. Frequency stabilization of quantum cascade laser for spectroscopic CO_2 isotope analysis. Infrared Phys. Techn. **2018**, *91*, 37-45.

(10) Nikodem, M.; Gomółka, G.; Klimczak, M.; Pysz, D.; Buczyński, R. Demonstration of mid-infrared gas sensing using an anti-resonant hollow core fiber and a quantum cascade laser. *Opt. Express* **2019**, *27*, 36350-36357.

(11) Zhou, T.; Wu, T.; Wu, Q.; Chen, W.; Wu, M.; Ye, C.; He, X. Real-time monitoring of ^{13}C-and ^{18}O-isotopes of human breath CO_2 using a mid-infrared hollow waveguide gas sensor. *Anal. Chem*. **2020**, *92*, 12943-12949.

(12) Li, Z.; Wang, Z.; Yang, F.; Jin, W.; Ren, W. Mid-infrared fiber-optic photothermal interferometry. *Opt. Lett*. **2017**, *42*, 3718-3721.

(13) Chen, J.; Hangauer, A.; Strzoda, R.; Fleischer, M.; Amann, M. C. Low-level and ultralow-volume hollow waveguide based carbon monoxide sensor. *Opt. Lett*. **2010**, *35*, 3577-3579.

(14) Wu, T.; Kong, W.; Wang, M.; Wu, Q.; Chen, W.; Ye, C.; He, X. Compact Hollow Waveguide Mid-Infrared Gas Sensor For Simultaneous Measurements of Ambient CO_2 and Water Vapor. *J. Lightwave Technol*. **2020**, *38*, 4580-4587.

(15) Dong, L.; Yin, W.; Ma, W.; Jia, S. A novel control system for automatically locking a diode laser frequency to a selected gas absorption line. *Meas. Sci. Technol*. **2007**, *18*, 1447-1452.

(16) Gong, P.; Xie, L.; Qi, X. Q.; Wang, R. A. QEPAS-based central wavelength stabilized diode laser for gas sensing. *IEEE Photonics Technol. Lett*. **2014**, *27*, 545-548.

(17) Wang, Q.; Wang, Z.; Ren, W. Wavelength-stabilization-based photoacoustic spectroscopy for methane detection. *Meas. Sci. Technol.* **2017**, 28, 065102.
(18) Kluczynski, P.; Axner, O. Theoretical description based on Fourier analysis of wavelength-modulation spectrometry in terms of analytical and background signals. *Appl Opt.* **1999**, *38*, 5803-5815.
(19) Westberg, J.; Wang, J.; Axner, O. Fast and non-approximate methodology for calculation of wavelength-modulated Voigt lineshape functions suitable for real-time curve fitting. *J. Quant. Spectrosc. Radiat. Transf.* **2012**,*113*, 2049-2057.
(20) Kluczynski, P.; Gustafsson, J.; Lindberg, Å. M.; Axner, O. Wavelength modulation absorption spectrometry—an extensive scrutiny of the generation of signals. *Spectrochim. Acta B* **2001**, *56*, 1277-1354.
(21) Kasyutich, V. L.; Martin, P. A. $^{13}CO_2/^{12}CO_2$ isotopic ratio measurements with a continuous-wave quantum cascade laser in exhaled breath. *Infrared Phys. Techn.* **2012**, *55*, 60–66.
(22) Miller, J. B.; Tans, P. P.; White, J. W. C.; Conway, T. J.; Vaughn, B. W. The atmospheric signal of terrestrial carbon isotopic discrimination and its implication for partitioning carbon fluxes. *Tellus B* **2003**, *55*, 197-206.
(23) Zahn, A.; Neubert, R.; Platt, U. Fate of long-lived trace species near the northern hemispheric tropopause: 2. Isotopic composition of carbon dioxide ($^{13}CO_2$, $^{14}CO_2$, and $C^{18}O^{16}O$). *J. Geophys. Res.* **2000**, *105*, 6719.
(24) King, C.-Y.; Koizumi, N.; Kitagawa, Y. Hydrogeochemical anomalies and the 1995 Kobe Earthquake. *Science* **1995**, *269*, 38.

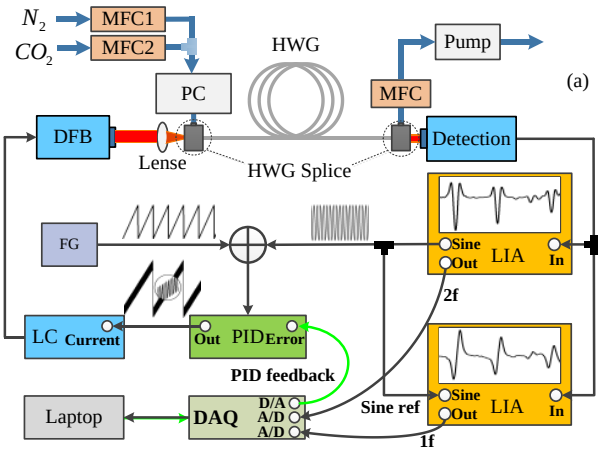

For Table of Contents Only